



University of
Massachusetts
Amherst

Investigation on Reaction Pathways for ZnO Formation from Diethylzinc and Water during Chemical Vapor Deposition

Item Type	article
Authors	Kim, Yong-Seok; Won, Yong-Sun
Download date	2026-05-13 04:23:12
Link to Item	https://hdl.handle.net/20.500.14394/38280

Investigation on Reaction Pathways for ZnO Formation from Diethylzinc and Water during Chemical Vapor Deposition

Young Seok Kim* and Yong Sun Won†*

Department of Chemical Engineering, University of Massachusetts, Amherst, MA 01003, USA

*E-mail: yskim@engin.umass.edu

†Samsung Electro-Mechanics, Central R&D Institute, Suwon, Gyeonggi-Do 443-743, Korea

*E-mail: yongsun.won@samsung.com

Received May 4, 2009, Accepted May 26, 2009

A computational study of the reactions between Zn-containing species, the products of the thermal decomposition of diethylzinc (DEZn) and water was investigated. The Zn-containing species – $\text{Zn}(\text{C}_2\text{H}_5)_2$, HZnC_2H_5 , and $(\text{ZnC}_2\text{H}_5)_2$ – were assumed to react with water during ZnO metal organic chemical vapor deposition (MOCVD). Density functional theory (DFT) calculations at the level of B3LYP/6-311G(d) were employed for the geometry optimization and thermodynamic property evaluation. As a result dihydroxozinc, $\text{Zn}(\text{OH})_2$, was the most probable reaction product common for all three Zn-containing species. A further clustering of $\text{Zn}(\text{OH})_2$ was investigated to understand the initial stage of ZnO film deposition. In experiments, the reactions of DEZn and water were examined by *in-situ* Raman scattering in a specially designed MOCVD reactor. Although direct evidence of $\text{Zn}(\text{OH})_2$ was not observed, some relevant reaction intermediates were successfully detected to support the validity of the gas phase reaction pathways proposed in the computational study.

Key Words: ZnO, Diethylzinc, Water, Reaction pathway, CVD

Introduction

The wide band gap energy of ZnO (3.4 eV) makes it useful in various optical applications such as light emitting diodes (LEDs), flat panel displays and solar cells. ZnO thin films are also used as the electrode of transparent conducting oxide (TCO) as a promising alternative to the more expensive indium tin oxide (ITO) films.^{1–4} Thin films of ZnO can be deposited by metal organic chemical vapor deposition (MOCVD) using various metal organic precursors^{5–7} and MOCVD is especially attractive for fabricating large scale devices, due to its high deposition rate and excellent thickness uniformity.

For MOCVD, the substrate selection is a critical decision. Although high quality bulk ZnO substrates are now under development, their high cost and limited availability preclude their use in mass production. Silicon is an attractive substrate because of its low cost, high crystallinity, availability of large sizes and wide range of thermal conductivity. For applications requiring transparent substrates, glasses and polymers are often used particularly for flexible displays.^{8–9} For those applications, the MOCVD temperature must be lower than the transition temperature of the substrates (e.g., glass transition temperature or melting point). To design the MOCVD reactor and optimize its deposition conditions especially constrained with a limited growth temperature for polymer substrates, better understanding of the gas phase reactions is required because the growth temperature in MOCVD is often determined by kinetically limited gas phase reactions.^{10–12}

In this study, the reactions of diethylzinc (DEZn) with water to form ZnO were investigated. A previous study demonstrated that homogeneous pyrolysis of DEZn produces two reaction intermediates, HZnC_2H_5 and $(\text{ZnC}_2\text{H}_5)_2$.¹¹ The former is formed from the β -hydride elimination of DEZn and

the latter by homolytic fission of the Zn-C bond in DEZn followed by dimerization. Therefore three Zn-containing species (i.e., two of the specified reaction intermediates and unreacted the DEZn) were considered as starting gas phase species for further reactions with water to form ZnO. With given information, a computational study based on DFT calculations aimed to clarify the most likely reaction pathway to ZnO by investigating the gas phase reactions and suggesting the pathways of ZnO cluster formation from resulting gas phase products. The *in-situ* Raman scattering technique was employed to detect gas phase reaction intermediates during the operation of a specially designed MOCVD reactor.

Methods

The computational calculations were performed using the *Gaussian 03* program package.¹³ Bond formation and dissociation energies were calculated using B3LYP-DFT model chemistry with 6-311G(d) basis set, based on the fully-optimized molecular geometries. The transition states were also located using the same model chemistry and basis set, enabling the evaluation of activation energies of the reaction pathways. Direct comparison of the calculated Gibbs energy changes was used in determining the likelihood of the gas phase reactions. The reaction temperature was assumed to be less than 600 °C as it allows for ZnO to be deposited on flexible substrates.^{8–9} Therefore the two specified reaction intermediates, HZnC_2H_5 and $(\text{ZnC}_2\text{H}_5)_2$, were regarded as Zn-containing reactants for further reactions with water in addition to unreacted DEZn.¹¹ At first, reactions of the three Zn-containing species with one water molecule were evaluated for the most likely product. Further reactions with another water molecule were considered to reach the end product,

Zn(OH)₂, which was used as a building block for ZnO cluster formation later on. This is valid since the concentration of water is much higher than that of metal organic species in a typical MOCVD.

To confirm the calculated results, a U-1000 Raman spectrometer (Jobin Yvon) was used to locate the reaction intermediates experimentally. The 532 nm wavelength of a Nd/YAG solid state laser was used as the excitation light source and a coupled charge device (CCD) was used as a detector. More detailed experimental procedures are explained elsewhere.¹¹

Results and Discussion

Reactions of Zn-containing species with water. The gas phase decomposition of DEZn in N₂ carrier gas demonstrated that 100% conversion did not occur under 600 °C. To deposit ZnO at low temperatures (e.g., onto polymer substrates), it is

necessary to examine the hydrolysis of unreacted DEZn. Figure 1[A] shows a reaction pathway of water attacking DEZn, which was first suggested by Smith and Schlegel using molecular orbital theory.¹⁴ The calculated results agree well with their results in terms of bond lengths and angles. The DEZn (1) has a linear C-Zn-C structure and the interatomic distance between the Zn and C is 2.04 Å. The Wiberg bond index from the natural bond orbital (NBO) analysis indicates that the most probable bond dissociation would take place at the Zn-C bond. In the case of the adduct of DEZn and water (2), the enthalpy was calculated to be 6.35 kcal/mol lower than that of the reactants. The Zn-C bond length slightly decreases to 1.96 Å and the linear arrangement of C-Zn-C shifts to an angle of 166.11°. Since Zn has an atomic charge of +2 in DEZn, it attracts the lone pairs of electrons of water to give a weak solvation effect thereby stabilizing the structure. Once the adduct (2) is formed, the hydrogen of water easily

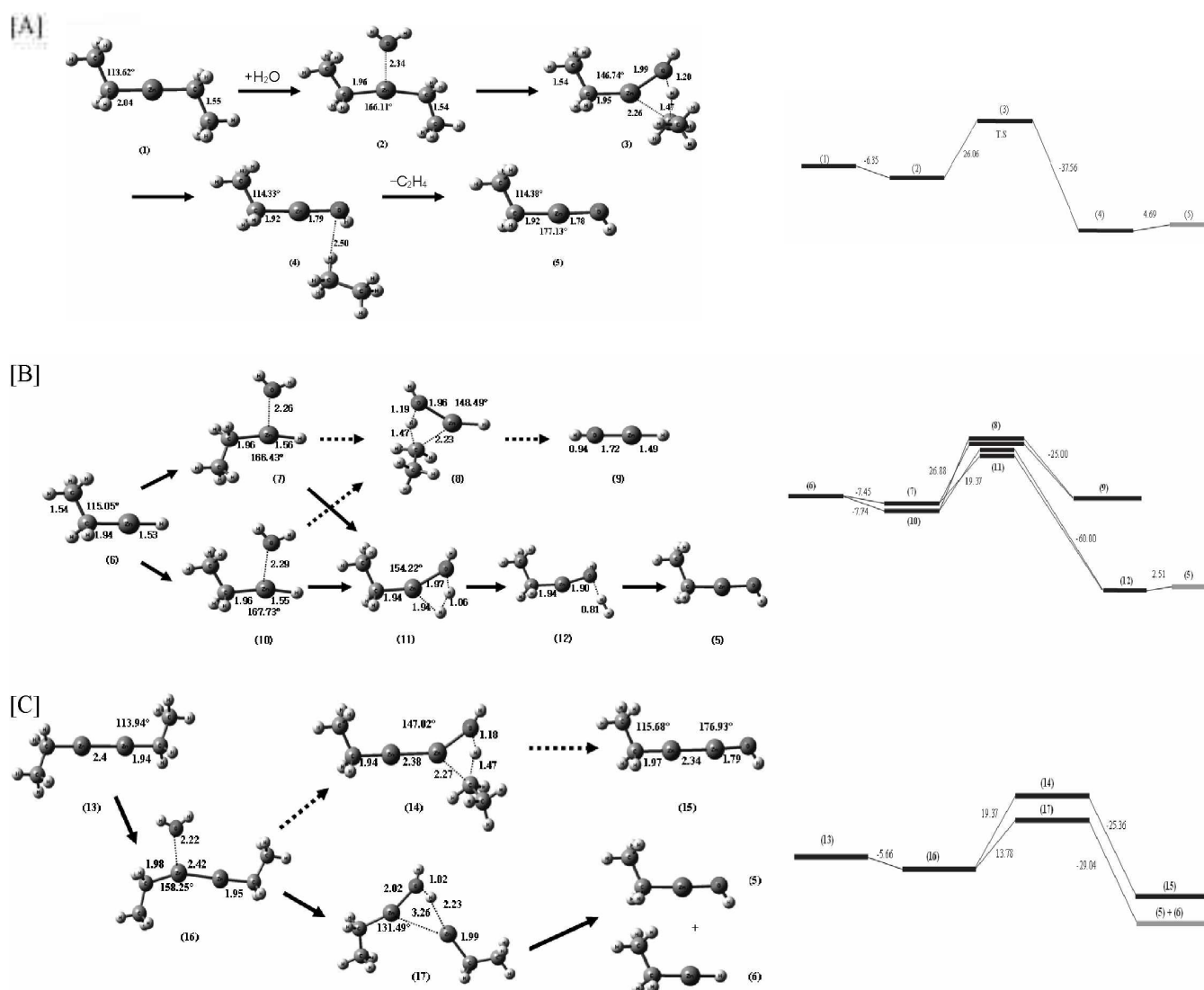


Figure 1. Possible reaction pathways and calculated energetics of DEZn [A], HZnC₂H₅ [B], and (ZnC₂H₅)₂ [C] with one molecule of water. Enthalpy changes have the unit of kcal/mol and bond lengths have the unit of Å. Dashed arrows indicate relatively unfavorable reaction pathways.

reacts with the nearby carbon. The transition state (3) shows a broad angle of 146.74° in the C-Zn-C arrangement with an elongated distance of 2.26 Å between the Zn and the C directly participating in the reaction. On the other hand, the distance between the Zn and the other C shortens to 1.95 Å, eventually converging to 1.92 Å in the reaction intermediates of (4) and (5). The pathway leads to the first important reaction intermediate (5) after the detachment of C_2H_6 from (4). The calculated energetics are also illustrated in Fig. 1.

Ethyl hydrido zinc (6), $HZnC_2H_5$, one of the reaction intermediates resulting from the thermal decomposition of DEZn, undergoes two possible reaction pathways with water as shown in Fig. 1[B]. At first, there are two molecular structures conceivable for the adduct of (6) and water, (7) and (10). However the enthalpies of (7) and (10) are approximately the same, which implies that C_2H_5 rotational barrier is negligible and thus they are energetically identical. Once water forms a weak coordinate covalent bond with Zn as in (7) and (10), two transition states of (8) and (11) are possible with respect to where the hydrogen of water attacks. The hydrogen attacks the ethyl group to release ethane as in (8) to yield hydrido hydrozinc (9) in one way. This intermediate (9) has a much shorter Zn-O bond length, since the bond characteristic has been changed from a coordinate covalent bond to a covalent

bond with the release of ethane. In the other way, the hydrogen of water attacks the innate hydrogen in (6) to release H_2 as in (11) and (12) to generate (5), the same ending structure as in Fig. 1[A]. It is interesting that DEZn and its decomposition product (6), which is generated *via* β -hydride elimination of DEZn, lead to the same reaction intermediate (5) when they combine with water. The corresponding enthalpy changes are also represented in Fig. 1. By comparing energetics of pathways [A] and [B], it is obvious that the ethyl hydrido zinc (6) is favorable in energy to arrive at (5) compared to DEZn.

The other reaction intermediate resulting from DEZn thermal decomposition, the dimer of monoethylzinc, $(ZnC_2H_5)_2$, is shown as (13) in Fig. 1[C]. The Zn-C bond length is shorter than that of DEZn, and free rotation of the ethyl groups is expected since the two carbons in (13) are separated by a large distance of 6.28 Å. The adduct of (13) and water is shown as (16), in which the C-Zn-Zn angle slightly bends to 158.25° as the water forms a coordinate covalent bond with Zn. Then two pathways are possible depending on the attack of the hydrogen of water, similar to Fig. 1[B]. When the hydrogen attacks the nearest carbon atom, it undergoes the transition state of (14) to release ethane and generate (15). This intermediate (15) can react further with another water to form $Zn(OH)_2$, which likely plays a key role in the formation of ZnO. However there is another more favorable reaction pathway than the one from (16) to (14). In (16), the hydrogen of water can react with the nearest Zn to go through the transition state of (17). The Zn-O bond length decreases due to the formation of a stronger bond, while the distance between the two Zn atoms increases from 2.42 Å to 3.26 Å. This reaction pathway is more favorable by ~ 5 kcal/mol than the other pathway (compare (17) to (14)). The end result of the pathway is (5) and (6). Coincidentally, the product (5) appears again in this pathway as well. In addition, the other product (6) would result in (5) by the reaction with another water as shown in Fig. 1[B].

Three reaction pathways are presented here to illustrate the complexity of the gas phase reactions of DEZn with water. The calculated geometric parameters, such as bond lengths and associated angles, are summarized in Table 1 for reference. It is noted that all the pathways produce ethyl hydrozinc (5) as a common reaction product. Another water would carry on a further reaction with (5) as shown in Fig. 2, which is energetically favorable as well. In fact, together with the three Zn-containing species – DEZn, (6), and (13) – and their products, it is anticipated that ZnH_2 is also present in the gas phase as a result of consecutive β -hydride eliminations of DEZn. This reaction product however was not considered in this study because it is expected to be thermodynamically stable only at

Table 1. Calculated geometric parameters of reaction species shown in Fig. 1

Structure	Bond Length (Å)				Angle ($^\circ$)
	Zn-O	Zn-C	Zn-H	Zn-Zn	
1	-	2.04	-	-	C-Zn-C: 180.00
2	2.34	1.96	-	-	C-Zn-C: 166.11
3	1.99	1.95	-	-	C-Zn-O: 146.74
4	1.79	1.92	-	-	C-Zn-O: 176.68
5	1.78	1.92	-	-	C-Zn-O: 177.13
6	-	1.94	1.53	-	C-Zn-H: 179.64
7	2.26	1.96	1.56	-	C-Zn-H: 166.43
8	1.96	2.23	1.53	-	O-Zn-H: 148.49
9	1.72	-	1.49	-	O-Zn-H: 179.34
10	2.29	1.96	1.55	-	C-Zn-H: 167.73
11	1.97	1.94	1.94	-	C-Zn-O: 154.22
12	1.90	1.94	-	-	C-Zn-O: 158.87
13	-	1.94	-	2.40	C-Zn-Zn: 179.63
14	1.99	1.94	-	2.38	C-Zn-Zn: 179.69
15	1.79	1.97	-	2.34	Zn-Zn-O: 176.93
16	2.22	1.98	-	2.42	C-Zn-Zn: 158.25
17	2.02	1.99	2.23	3.26	C-Zn-Zn: 131.49

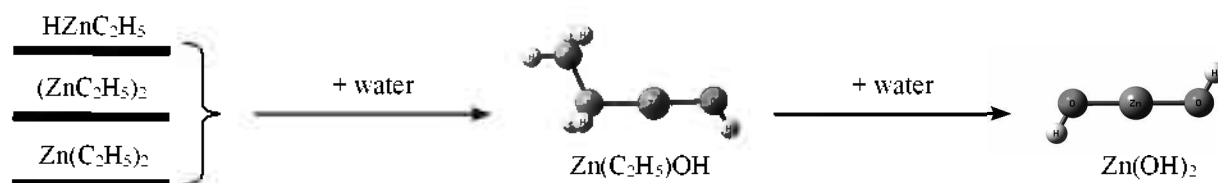


Figure 2. Proposed reaction pathways of three Zn-containing species and water.

temperatures above 650 °C. Moreover, when ZnH_2 exists in the gas phase with excess water, it follows a similar reaction pathway as that shown in Fig. 1 to produce the same product, $\text{Zn}(\text{OH})_2$.

ZnO formation. ZnO film has a wurtzite structure with lattice parameters of $a = 3.250$ and $c = 5.207$ Å. The ZnO deposition *via* surface reactions is beyond the scope of this study, but it is necessary to consider formation of ZnO clusters to get insight of ZnO formation on the surface. The building block for clusters is dihydroxozinc (18), which is the common end product of the reactions between Zn-containing species and water as discussed in the preceding section. Previously meta-stable Zn_2O_2 , Zn_3O_3 and Zn_4O_4 were examined as ZnO initiating structures,¹⁵⁻¹⁶ but these molecules are ideal 2-dimensional structures, which can accept additional Zn and O atoms to expand their structures into 3-dimensional forms. Similarly, we suggested the assembly of two or three dihydroxozinc (18) monomers as shown in Fig. 3 along with calculated energetics.

The pathway in Fig. 3[A] represents the dimerization of two (18) monomers. Two Zn and two O atoms form a ring structure at the center due to the weak solvation effect from the lone pairs electrons in the oxygens. In accordance, the Zn-O bond lengths at both sides are elongated slightly from 1.76 to 1.79 Å. The Zn-O bond lengths are not identical in the ring (1.91 and 1.95 Å) because the shorter is a coordinate covalent bond and the longer is formed by electrostatic interaction between Zn and O atoms. The dimer (19) then combines with another (19) to form a larger cluster (20). The Zn-O bond lengths of the dangling branches from the cubic structure of (20) are elongated again to 1.80 Å and the Zn-O bond lengths inside the cubic structure are increased to 2.02 and 2.04 Å. It is noted that the difference between the Zn-O bond lengths inside the cubic segment of (20) is reduced compared to that of (19): 0.04 Å (1.95 Å \rightarrow 1.91 Å) in (19) to 0.02 Å (2.04 Å \rightarrow 2.02 Å) in (20). It shows that the energy is dispersed into three directions because each atom of Zn or O in the cubic segment of (20) is interacting with three neighboring atoms. Near the

substrate surface, the clusters suggested in Fig. 3 possibly react with absorption sites to initiate ZnO film growth. The cluster, starting with the dimerization of $\text{Zn}(\text{OH})_2$ as in Fig. 3[A], however was not likely related to the formation of wurtzite structure.

Meanwhile, a ring formation with three (18) monomers having more favorable energetics (-87.9 kcal/mol compared to -49.3 kcal/mol for dimerization) is possible as shown in Fig. 3[B]. The ring structure in (21) was a global minimum among other conceivable structures from three monomers. The Zn-O bond lengths in the dangling branches of (21) increase as the trimerization progresses, similar to the pathway in Fig. 3[A]. The trimer (21) is 2-dimensional but the products of the clustering of (21) are 3-dimensional as in (22) and (23). The structure (23) is composed of two layers of (21). The three Zn atoms in the first layer are bonded with three O atoms in the second layer and vice versa. The distance between the two layers of (23) is 2.18 Å and the Zn-O bonds in the upper or bottom layer are slightly elongated compared to those in (22). The elongation of Zn-O bonds would continue as further assembly proceeds with building blocks of (18). Therefore, the structures with more building blocks of (18) combined onto (23) would give closer values to the Zn-O bond length corresponding to the experimental lattice parameters of the ZnO wurtzite structure ($a = 3.250$ and $c = 5.207$ Å). In fact, Behnman reported that the ZnO cluster has the stable spheroid structure when the numbers of Zn and O atoms is greater than 11.¹⁶

Table 2 summarizes the calculated Gibbs energy changes for the reactions given in Fig. 3 at 600 °C and enthalpy changes at 25 °C. The negative signs in the Gibbs energy changes indicate that both pathways are spontaneous and the trimerization is more favorable than dimerization by the difference of the absolute values. The Gibbs energy changes could be a clue as to which reactions are more favorable during MOCVD. Again, the negative Gibbs energy change implies that the reaction is stable in the gas phase. Meanwhile, the positive

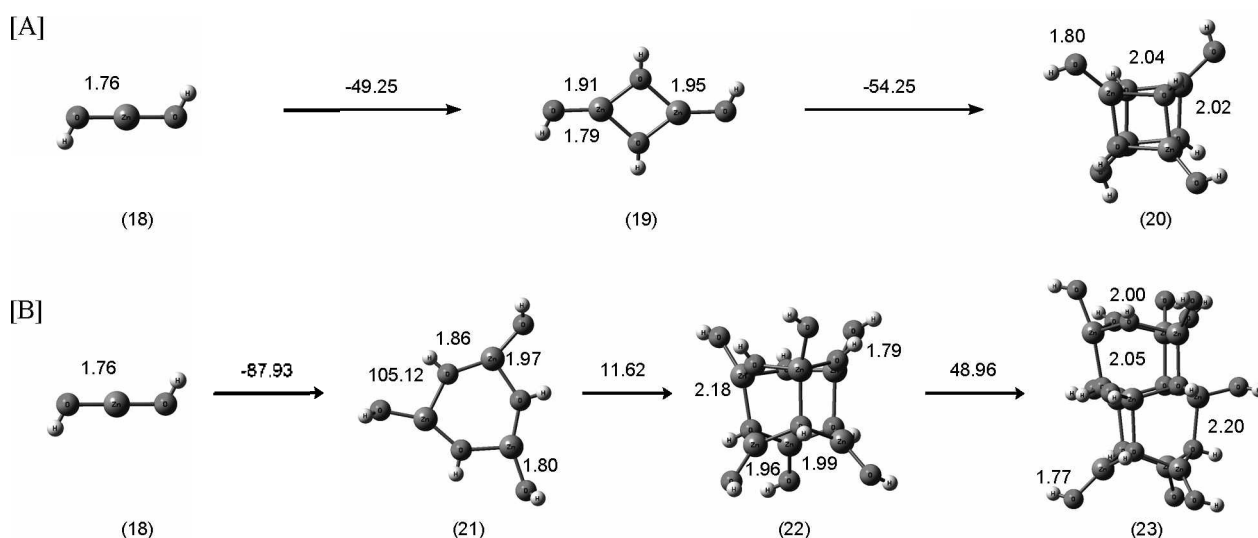


Figure 3. Possible reaction pathways of $\text{Zn}(\text{OH})_2$ clustering starting with dimerization [A] and trimerization [B]. The enthalpy changes have the unit of kcal/mol.

Gibbs energy change indicates that the reaction, such as (21) \rightarrow (22) or (22) \rightarrow (23), is not likely to occur in the gas phase. Thus, the formation of wurtzite ZnO structure is initiated based on the cluster species (21) formed in the gas phase and adsorbed onto the substrate surface. Then additional assembly of building blocks leads to a nucleus having wurtzite structure inside as in (23) in a logical way.

The comparison of the dipole moments of the cluster species gives additional support to this proposition. The dipole moment increases during the dimerization and trimerization of $\text{Zn}(\text{OH})_2$, (18) \rightarrow (19) and (18) \rightarrow (21) respectively. However, it decreases in (19) \rightarrow (20), because the cluster (20) evolves into a more symmetrical 3-dimensional form. Meanwhile, the dipole moment keeps increasing drastically during clustering, (21) \rightarrow (22) \rightarrow (23), as in Fig. 3 (b). Once formed on the substrate surface, the cluster species, (22) and (23), having a very large dipole moment, attract gas phase molecules to enhance further clustering and develop nuclei for the ZnO film deposition.

Identification of reaction intermediates using *in situ* Raman spectroscopy. Important experiments probing the decom-

Table 2. Calculated Gibbs energy and enthalpy changes of the reactions in Fig. 3 and the dipole moments of the species involved; the Gibbs energy and enthalpy changes have the unit of kcal/mol and the dipole moments have the unit of Debye

Reactions	ΔH_{298}	ΔG_{298}	Dipole moment	
(18) \rightarrow (19)	-49.25	-15.99	(18)	0.00
(19) \rightarrow (20)	-54.25	-12.73	(19)	0.19
			(20)	0.02
(18) \rightarrow (21)	-87.93	-24.56	(21)	3.90
(21) \rightarrow (22)	11.62	94.35	(22)	8.87
(22) \rightarrow (23)	48.96	137.83	(23)	26.51

position of DEZn with Raman spectroscopy revealed the primary decomposition products, ZnH_2 and $\text{Zn}(\text{C}_2\text{H}_5)_2$.¹¹ Based on this observation, computational calculations were performed to evaluate the most likely reaction pathways between the Zn-containing species and water in the preceding sections. Thus experiments were conducted to detect the calculated intermediate species. In the experiments, 0.1 mol% of DEZn was diluted in a N_2 carrier gas and introduced through the center line of the specially designed MOCVD reactor.¹¹ At the same time, 0.1 mol% of water was introduced into a separate gas inlet. The two gas streams were mixed just before the reactor inlet. The other gas inlets, annular and sweep inlets, flowed only N_2 carrier to envelop the DEZn/water gas flow, and therefore kept the mixture gas flow isolated from any surface making perfect homogeneous reaction conditions. The reactor was then brought to the steady state and the centerline (the mixture gas flow) was probed by Raman scattering in search of molecular vibrational motions. All flow velocities were controlled to avoid recirculation, and the heater was set at 600 °C. Figure 4 shows the Raman spectra in the range of the expected peaks of the species shown in Fig. 1. Four dominant peaks were found in the range of 270 to 420 cm^{-1} . The temperature denoted on each spectrum was obtained from the observed N_2 rotational spectra. In fact, the actual heater temperature was extrapolated based on these temperatures.¹¹

At first glance, there are three dominant peaks near the substrate (see the uppermost spectrum), which began to develop at ~ 300 °C. A fourth peak was detected at 311 cm^{-1} but only at an estimated temperature of 315 °C. Although the signal for these peaks was low, they provide indirect evidence of the reaction pathways. Figure 4 also shows peak assignments. The first peak at 280 cm^{-1} can be assigned to the OH

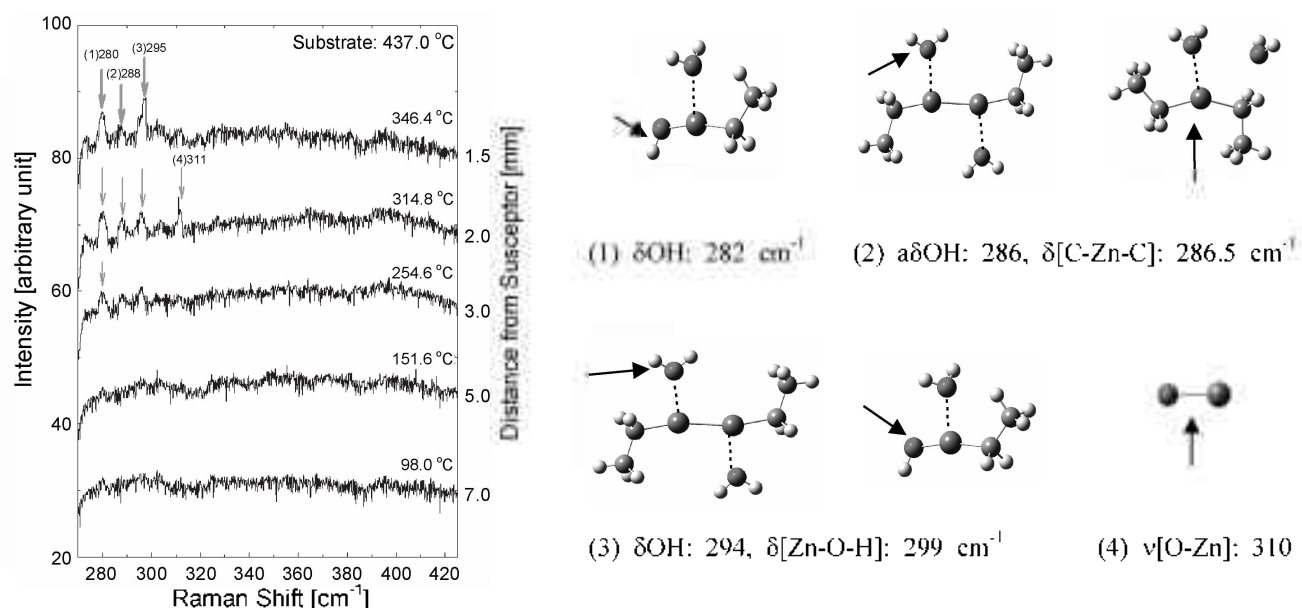


Figure 4. (Left) Raman spectra taken at various positions (temperatures) using 532 nm laser source. The probing beam was focused at the central gas flow. The heater temperature was set at 600 °C and the temperature gradient of gas stream was formed by radiation heating. Temperature at each position was experimentally determined from the Boltzmann distribution of the rotational spectra of the rotational spectra of N_2 carrier gas. (Right) Possible vibrational motions assigned for detected peaks. Four peaks were observed above 255 °C.

bending motion of the molecule which is formed by the reaction of (5) with another water. The species (5) is the product from all three reaction pathways as shown in Fig. 1. The second peak at 288 cm^{-1} may be related to either one of the two species. One is an adduct of (13) and two water molecules resulting in asymmetrical OH bending and stretching which has a frequency of 286 cm^{-1} as shown in Fig. 4. Otherwise the C-Zn-C bending of an adduct of DEZn and two water molecules also has the frequency of 286.5 cm^{-1} . It represents the possibility of the pathways in Fig. 1[A] and [C]. The peak at 295 cm^{-1} is likely assigned to the symmetrical OH stretching of water in the adduct of (13) and two water molecules. It is also applicable for the Zn-O-H symmetrical bending motion in the adduct of (5) and water. Finally, the peak at 311 cm^{-1} is probably assigned to Zn-C stretching of ZnO fragment from any unstable molecule. The relative Raman cross-section of DEZn is very small and correspondingly its reaction intermediates may have small cross-sections as well. It implies the difficulty of detection and thus the direct revealing of the reaction pathways.

Conclusions

The reactions of three Zn-containing species – $\text{Zn}(\text{C}_2\text{H}_5)_2$, HZnC_2H_5 , and $(\text{ZnC}_2\text{H}_5)_2$ – and water were investigated. DFT calculations at the level of B3LYP/6-311G(d) were employed to optimize molecular structures and locate transition states. Three possible reaction pathways led to ethyl hydrido zinc, $\text{ZnC}_2\text{H}_5\text{OH}$, which further proceeded to dihydrido zinc, $\text{Zn}(\text{OH})_2$, with additional water. With that $\text{Zn}(\text{OH})_2$ plays a key role in the deposition of wurtzite ZnO film, further self-assembly reactions have been suggested. A ring species is formed from three $\text{Zn}(\text{OH})_2$ monomers and its further assembly leads to a ZnO cluster having wurtzite structure.

The experiments were prepared in a specially designed MOCVD reactor with DEZn and water as precursors to detect the reactant intermediates suggested in the computational study by using *in-situ* Raman spectroscopy. Although the direct evidence of dihydrozinc was not attained due to the fast reaction kinetics and relatively small Raman cross-sections of DEZn derivatives, some relevant reaction intermediates were detected to support the validity of the computationally proposed gas phase reaction pathways.

References

- Bachari, E. M.; Baud, G.; Amor, S. B.; Jacquet, M. *Thin Solid Films* **1999**, *348*, 165.
- Waag, A.; Gruber, Th.; Thonke, K.; Sauer, T.; Kling, R.; Kirchner, C.; Röss, H. *J. Alloy. Compd.* **2004**, *371*, 77.
- Zeng, K.; Zhu, F.; Hu, J.; Shen, L.; Zhang, K.; Gong, H. *Thin Solid Films* **2003**, *443*, 60.
- Feng, X. *J. Phys.: Condens. Matter* **2004**, *16*, 4251.
- Wang, L.; Pu, Y.; Chen, Y. F.; Mo, C. L.; Fang, W. Q.; Xiong, C. B.; Dai, J. N.; Jiang, F. Y. *J. Cryst. Growth* **2004**, *284*, 459.
- Haga, K.; Katahira, F.; Watanabe, H. *Thin Solid Films* **1999**, *343*, 145.
- Mycielski, A.; Kowalczyk, L.; Szadkowski, A.; Chwalisz, B.; Wyszniak, A.; Stepniowski, R.; Baranowski, J. M.; Petemski, M.; Witowski, A.; Jakiela, R.; Barcz, A.; Witkowska, B.; Kaliszek, W.; Jedrzejczak, A.; Suchocki, A.; Lusakowska E.; Kaminska, E. *J. Alloy. Compd.* **2004**, *371*, 150.
- Allendorf, M. D. *Thin Solid Films* **2001**, *392*, 155.
- Chandrasekhar, R.; Choy, K. L. *Thin Solid Films* **2001**, *398*, 59.
- Allendorf, M. D.; Melius, C. F. *Surf. Coat. Technol* **1998**, *108*, 191.
- Kim, Y. S.; Won, Y. S.; Weaver, H.; Omenetto, N.; Anderson, T. *J. J. Phys. Chem. A* **2008**, *112*, 4246.
- Won, Y. S.; Kim, Y. S.; Kryliouk, O.; Anderson, T. *J. J. Cryst. Growth* **2008**, *310*, 3735.
- Frisch, M. J.; Trucks, G. W.; Schlegel, H. B.; Scuseria, G. E.; Robb, M. A.; Cheeseman, J. R.; Montgomery, J. A.; Vreven, T.; Kudin, K. N.; Burant, J. C.; Millam, J. M.; Iyengar, S. S.; Tomasi, J.; Barone, V.; Mennucci, B.; Cossi, M.; Scalmani, G.; Rega, N.; Petersson, G. A.; Nakatsuji, H.; Hada, M.; Ehara, M.; Toyota, K.; Fukuda, R.; Hasegawa, J.; Ishida, M.; Nakajima, T.; Honda, Y.; Kitao, O.; Nakai, H.; Klene, M.; Li, X.; Knox, J. E.; Hratchian, H. P.; Cross, J. B.; Bakken, V.; Adamo, C.; Jaramillo, J.; Gomperts, R.; Stratmann, R. E.; Yazyev, O.; Austin, A. J.; Cammi, R.; Pomelli, C.; Ochterski, J. W.; Ayala, P. Y.; Morokuma, K.; Voth, G. A.; Salvador, P.; Dannenberg, J. J.; Zakrzewski, V. G.; Dapprich, S.; Daniels, A. D.; Strain, M. C.; Farkas, O.; Malick, D. K.; Rabuck, A. D.; Raghavachari, K.; Foresman, J. B.; Ortiz, J. V.; Cui, Q.; Baboul, A. G.; Clifford, S.; Cioslowski, J.; Stefanov, B. B.; Liu, G.; Liashenko, A.; Piskorz, P.; Komaromi, I.; Martin, R. L.; Fox, D. J.; Keith, T.; Al-Laham, M. A.; Peng, C. Y.; Nanayakkara, A.; Challacombe, M.; Gill, P. M. W.; Johnson, B.; Chen, W.; Wong, M. W.; Gonzalez, C.; Pople, J. A. *Gaussian 03 Revision C.02*; Gaussian, Inc.: Wallingford CT, 2004.
- Smith, S. M.; Schlegel, H. B. *Chem. Mater.* **2003**, *15*, 162.
- Matyain, J. M.; Fowler, J. E.; Ugalde, J. M. *Phys. Rev. A* **2002**, *62*, 053201.
- Behrman, E. C.; Foehrweiser, R. K.; Myers, J. R.; French, B. R.; Zandler, M. E. *Phys. Rev. A* **1994**, *49*, R1543.